Cell Reports
Physical Science

CellPress
OPEN ACCESS

Article

Effective Photon Management of Non-Surface-Textured Flexible Thin Crystalline Silicon Solar Cells

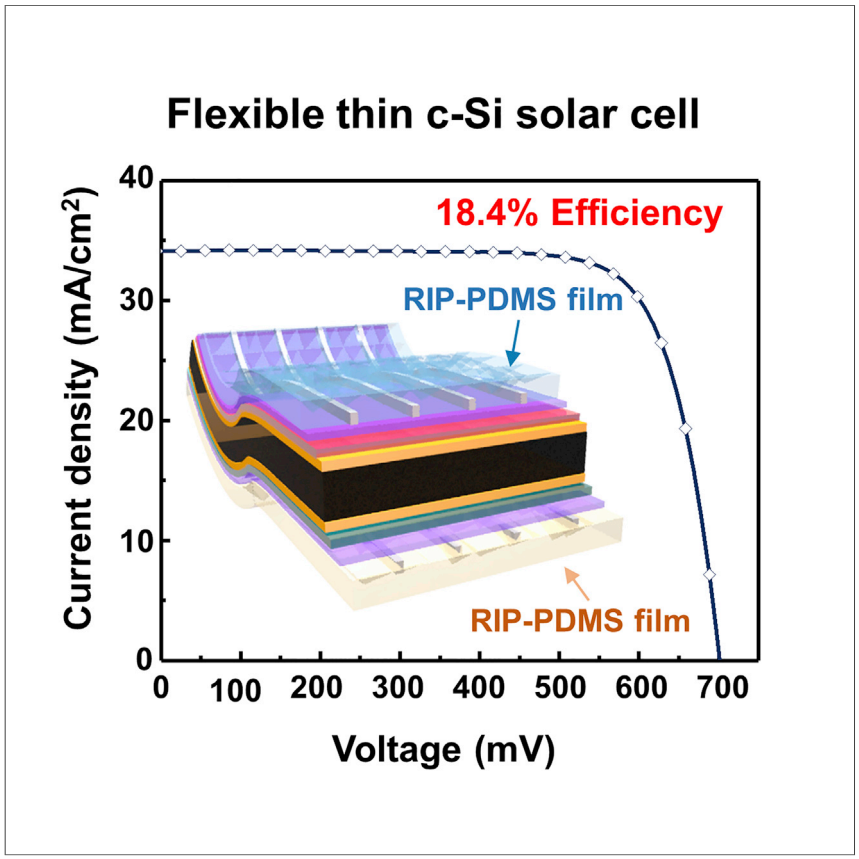

Hwang et al. develop highly efficient flexible solar cells by employing a random inverted pyramidal-polydimethylsiloxane (RIP-PDMS) film. Remarkably, thin c-Si solar cells with the RIP-PDMS films exhibit an efficiency of 18.4%, and their efficiency remains stable under 1,000 cycles of bending at a bending radius of less than 10 mm.

Inchan Hwang, Youngsoon Jeong, Yuta Shiratori, Jeonghwan Park, Shinsuke Miyajima, Ilsun Yoon, Kwanyong Seo

miyajima.s.aa@m.titech.ac.jp (S.M.)
ilsunyoon@cnu.ac.kr (I.Y.)
kseo@unist.ac.kr (K.S.)

HIGHLIGHTS

RIP-PDMS films improve the light absorption of the thin c-Si solar cells

Thin c-Si solar cells with RIP-PDMS films show efficiency of up to 18.4%

Thin c-Si solar cells with RIP-PDMS films show outstanding flexibility

Hwang et al., Cell Reports Physical Science 1, 100242
November 18, 2020
https://doi.org/10.1016/j.xcrp.2020.100242

Cell Reports
Physical Science

CellPress
OPEN ACCESS

Article

Effective Photon Management of Non-Surface-Textured Flexible Thin Crystalline Silicon Solar Cells

Inchan Hwang,[1,4] Youngsoon Jeong,[2,4] Yuta Shiratori,[3] Jeonghwan Park,[1] Shinsuke Miyajima,[3,*] Ilsun Yoon,[2,*] and Kwanyong Seo[1,5,*]

SUMMARY

Thin crystalline silicon (c-Si) showing outstanding flexibility has been considered as an active material for flexible solar cells. However, an effective photon management should be developed for thin c-Si, which shows severe light absorption loss. Here, we introduce random inverted-pyramidal polydimethylsiloxane (RIP-PDMS) films on the surface of the thin c-Si solar cell to simultaneously secure high absorption and flexibility. Attaching the RIP-PDMS film on the front surface of the device can significantly reduce surface reflection; near-infrared light recycling can be further improved by attaching a metal-coated RIP-PDMS film on the rear surface of the device. Notably, thin c-Si solar cells with RIP-PDMS films have an efficiency of 18.4% and exhibit a constant efficiency during 1,000 repeated bending tests with a bending radius of 10 mm. Also, finite-difference time-domain simulations confirm that the RIP-PDMS films increase the light diffusion and optical path length inside the c-Si.

INTRODUCTION

Lightweight and flexible solar cells are gaining considerable attention as continuous power sources that can be integrated with electronic devices. Among various types of solar cells, those based on crystalline silicon (c-Si) have been successfully commercialized, owing to their high efficiency of 26.7%, long-lifespan of more than 20 years, and mature manufacturing process.[1] However, the commercialized c-Si solar cells based on c-Si with a thickness of 150 μm or more for efficient light absorption are ineffective for releasing the mechanical stress due to their rigidity.[2] Therefore, the commercialized c-Si solar cells are limited to be employed as flexible solar cells because their efficiency dramatically degrades due to the generation of cracks when they are installed on curved or uneven surfaces. Recently, the fabrication of thin c-Si solar cells with less than 50-μm-thick c-Si substrates has been attempted to realize flexible solar cells by reducing their rigidity.[2–7] The resulting thin c-Si solar cells have the advantages of high flexibility, light weight, and excellent price competitiveness.[4] Furthermore, thin c-Si flexible solar cells can be manufactured based on the conventional fabrication process of the c-Si solar cell; therefore, they are expected to be commercialized quickly.[7]

To realize high-efficiency flexible thin c-Si solar cells, their light absorption should be improved through photon management. A thin c-Si layer without anti-reflection treatment shows an extreme light absorption loss of more than 30% in the entire wavelength range of 300–1,100 nm because of the refractive index mismatch

[1]School of Energy and Chemical Engineering, Ulsan National Institute of Science and Technology (UNIST), Ulsan 44919, Republic of Korea

[2]Department of Chemistry, Chungnam National University, Daejeon 34134, Republic of Korea

[3]Department of Electrical and Electronic Engineering, Tokyo Institute of Technology, Meguro, Tokyo 152-8550, Japan

[4]These authors contributed equally

[5]Lead Contact

*Correspondence: miyajima.s.aa@m.titech.ac.jp (S.M.), ilsunyoon@cnu.ac.kr (I.Y.), kseo@unist.ac.kr (K.S.)

https://doi.org/10.1016/j.xcrp.2020.100242

between air and c-Si. Moreover, thin c-Si exhibits drastic absorption loss at wavelengths exceeding 900 nm due to its low absorption coefficient.[8] Because the sunlight in the long-wavelength region exceeding 900 nm constitutes about 18% of the solar radiation energy, the absorption of such long-wavelength light by the thin c-Si solar cells should be improved for achieving high efficiency. Recently, nano/micro surface structures have been formed on thin c-Si solar cells to increase their absorption property.[3,5,9–13] With nano-/microstructures, thin c-Si solar cells with a thickness of 50 μm showed outstanding efficiency of 18.9%.[2] Although nano-/microstructures can effectively increase the light absorption by thin c-Si solar cells, issues such as the complicated fabrication process and severe recombination of minority carriers persist.[14] In particular, the surface structures could act as crack initiation sites where the mechanical stress can concentrate.[2,15] Such crack initiation sites would significantly degrade the flexibility of the thin c-Si solar cells. Hence, the development of a new light-trapping strategy is required to improve light absorption in the entire wavelength region while maintaining the stable flexibility of the thin c-Si solar cells.

In this work, a random inverted-pyramidal polydimethylsiloxane (RIP-PDMS) film is employed on thin c-Si solar cells as a means of effective photon management. The thin c-Si solar cell with RIP-PDMS films shows an improved integrated photon flux (85.4%) than that of the bare thin c-Si solar cell (75.0%) because of the enhanced light absorption in the entire wavelength range from 300 to 1,100 nm. Through finite-difference time-domain (FDTD) simulations, we confirmed that the RIP-PDMS films can improve the light absorption by the thin c-Si solar cells by allowing the elongation of the optical path length of the incident light, which can be elucidated from the tilting of the angles of the refracted light at the front and rear surfaces of the thin c-Si layer up to 10° and 15°, respectively. Upon attaching the RIP-PDMS films, the thin c-Si solar cell manufactured by a doping process shows an increased efficiency of 17.3% than that of the same device without the RIP-PDMS film (14.5% efficiency). Furthermore, the heterojunction with intrinsic thin layer (HIT) thin c-Si solar cells with RIP-PDMS films exhibits a maximum efficiency of 18.4%. In particular, our thin c-Si flexible solar cells with the RIP-PDMS optical films remain stable under bending without any change in efficiency, even when subjected to 1,000 bending cycles at a bending radius of less than 10 mm. Thus, we believe that thin c-Si with RIP-PDMS optical films could be a promising candidate for highly efficient flexible solar cells.

RESULTS

Flexible and Optical Characteristics of Thin c-Si

The bending radius ($R_{bending}$) of a c-Si substrate is proportional to its thickness, according to the following relationship:[2,16]

$$R_{bending} = \frac{ET}{2S} \quad \text{(Equation 1)}$$

Here, E is the modulus of elasticity, T is the thickness of the c-Si substrate, and S is the tensile yield strength. A decrease in $R_{bending}$ implies an increase in the flexibility of c-Si. In this study, we considered a free-standing, 20-μm-thin c-Si as the starting material, which is theoretically capable of achieving more than 20% efficiency.[17–19] The 20-μm-thin c-Si substrate exhibits excellent flexibility with an $R_{bending}$ value of 5 mm, as demonstrated in Figure 1A. However, the bare thin c-Si substrate suffers from severe light absorption loss in the entire wavelength range of 300 to 1,100 nm, because the flat surface reflects more than 30% of the incident light. Moreover, the light absorption by c-Si drops significantly at wavelengths greater than 900 nm, owing to its low absorption coefficient (Figure 1B). Even if a silicon nitride

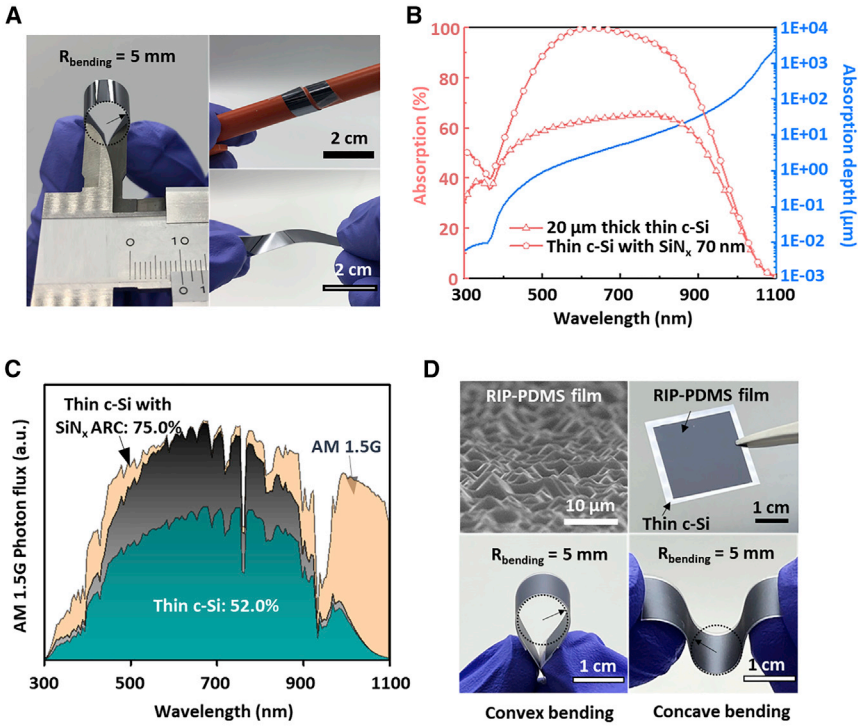

Figure 1. Flexible and Optical Characteristics of Thin c-Si

(A) Photographs of a thin c-Si substrate (20 μm thickness).

(B) Absorption spectra of thin c-Si with and without a 70-nm-thick SiN_x layer. The right y axis shows the absorption depth of the c-Si substrate.

(C) Spectral distribution of the photon flux of thin c-Si with and without the SiN_x layer (70 nm) and AM 1.5 G spectrum.

(D) Photographs and scanning electron micrograph of thin c-Si with an RIP-PDMS film under bending.

(SiN_x) anti-reflection layer (ARC) is coated on the surface of thin c-Si, the absorption of the thin c-Si substrate only increases in the limited wavelength region of 500–900 nm. As shown in Figure 1B, the severe absorption loss of thin c-Si at wavelengths greater than 900 nm can also be explained by the absorption depth, a parameter that indicates how deeply light penetrates a semiconductor before being absorbed. To clearly compare the light absorption loss of thin c-Si, the integrated photon flux was calculated based on Figure 1B, using Equation 2.

$$A(\lambda)_{\text{Integrated photon flux}} = \frac{\int_{300nm}^{1100nm} b(\lambda)A(\lambda)d\lambda}{\int_{300nm}^{1100nm} b(\lambda)d\lambda} \quad \text{(Equation 2)}$$

where $b(\lambda)$ is the photon flux density of the air mass 1.5 global (AM 1.5G) solar spectrum and $A(\lambda)$ is the wavelength-dependent absorption. The calculated integrated photon flux of bare thin c-Si is only 52.0% of the incident light (Figure 1C). When a SiN_x ARC is applied on the thin c-Si substrate, the integrated photon flux increases to 75.0%, indicating limited improvement in light absorption. Thus, to maximize the light absorption of thin c-Si solar cells, not only the ARC layer that reduces surface reflection but also surface structures that can increase the optical path length should be considered simultaneously.

In this study, the RIP-PDMS film was applied on the surface of thin c-Si solar cells with a SiN_x ARC layer to enhance the light absorption capability of the thin c-Si layer.

PDMS is an ideal material for an optical film, because it has high transmittance of >95%, low surface reflection of <3%, and it adheres excellently to c-Si.[20–23] In such a thin c-Si solar cell, the RIP surface structures of the PDMS film would increase the optical path length of c-Si. The RIP-PDMS films were fabricated by a soft lithography process using a c-Si master mold with micron-sized random pyramidal structures. As shown in Figure S1, the fabricated RIP-PDMS film showed a high transmittance (over 96%) and low intrinsic absorption (below 1%) over the entire measured wavelength range. The main advantage of attaching the RIP-PDMS film onto the thin c-Si solar cell rather than directly fabricating nano/micro surface structures on the surface is to prevent the generation of crack initiation sites in the thin c-Si layer. In general, the nano/micro surface structures possess crack initiation sites that can concentrate the mechanical stress, which can decrease the flexibility of the thin c-Si solar cells.[2] In contrast, the RIP-PDMS films do not generate crack initiation sites on the thin c-Si layer, because it is physically attached onto the surface of the thin c-Si solar cells. In other words, the thin c-Si solar cells with RIP-PDMS film can simultaneously show both stable flexibility and enhanced absorption. Because the RIP-PDMS film is highly adhesive to the c-Si surface and easily deforms elastically with the Poisson number of 0.5, it can effectively release the mechanical stress when the solar cell is deformed. Thus, a thin c-Si substrate with RIP-PDMS films shows excellent flexibility even at an $R_{bending}$ of 5 mm, as shown in Figure 1D.[19,24,25]

Experimental and FDTD-Simulated Optical Analysis of Thin c-Si with RIP-PDMS Films

To analyze the enhancement of the light absorption capability of the thin c-Si substrate with RIP-PDMS films, the absorption spectra of various devices with and without RIP-PDMS films were obtained as shown in Figure 2A. In all samples, except for those prepared with RIP-PDMS films on both front and rear surfaces, an Ag mirror with a thickness of 300 nm was placed on the rear surface of the c-Si layer to recycle the light passing through the thin c-Si layer. The absorbance $A(\lambda)$ of the samples was calculated using the relationship $A(\lambda) = 1 - R(\lambda)$, where $R(\lambda)$ is the reflectance. The reflectance of each sample was measured (see Figure S2), including specular and diffuse reflections, in the wavelength range of 300–1,100 nm using a ultraviolet-visible (UV-vis)-near infrared (NIR) spectrophotometer (Cary 5000, Agilent Technologies) equipped with an integrating sphere (diameter = 110 mm). By depositing a 300-nm-thick metal mirror layer on the rear surface of the thin c-Si substrate, we ensured that no light was transmitted through the sample. When an RIP-PDMS film is attached to the front surface of the thin c-Si substrate with a SiN_x ARC layer, the RIP-PDMS film (n = 1.4) decreases the refractive index difference between air (n = 1.0) and SiN_x (n = 2.0), thus significantly enhancing the light absorption by the thin c-Si at shorter wavelengths ($\lambda < 500$ nm), as shown in Figure 2A. Moreover, with the attachment of the RIP-PDMS film, the thin c-Si substrate shows improved absorption of light of longer wavelengths ($\lambda > 800$ nm). In addition, the thin c-Si with the RIP-PDMS film showed low surface reflection compared to that with the flat-PDMS film (Figure S3). Hence, it was verified that the surface structures on the PDMS film were required to effectively enhance the light trapping efficiency of the thin c-Si. Figure 2B shows the integrated photon flux of the thin c-Si; it confirms a significant enhancement in light absorption by the thin c-Si with an RIP-PDMS film on the front surface (82.1%) than that of a thin c-Si substrate without the RIP-PDMS film (75%). The RIP-PDMS film increases the angle of incidence of light entering into the thin c-Si through refraction on the inverted-pyramidal surface, thereby increasing the path length of light passing through the thin c-Si layer. Similar enhancement of light absorption facilitated by a PDMS film has been discussed in our previous report.[20] Despite the increase in light absorption facilitated by the RIP-PDMS film attached

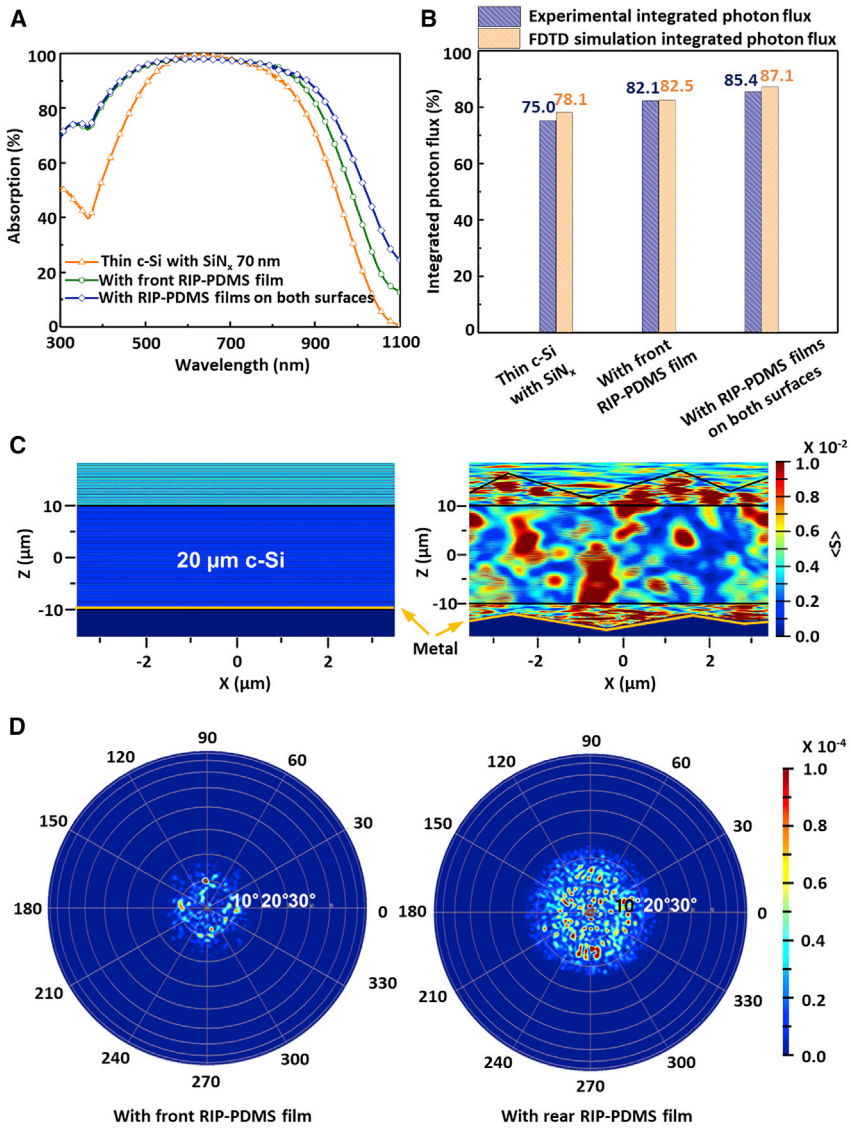

Figure 2. Experimental and FDTD-Simulated Optical Analysis of Thin c-Si with RIP-PDMS Films

(A) Experimental absorption spectra of SiN_x coated thin c-Si, the thin c-Si with an RIP-PDMS film on the front surface, and the thin c-Si with RIP-PDMS films on both front and rear surfaces. The structures of thin c-Si with RIP-PDMS films are shown in Figure S4.

(B) Comparison of the integrated photon flux obtained by FDTD simulation with the experimental value.

(C) Vertical cross-sections of the time-averaged Poynting vector of the thin c-Si calculated at λ = 1,000 nm with and without RIP-PDMS films.

(D) Far-field projections for describing light propagation in thin c-Si by attaching RIP-PDMS films to both the front and rear surfaces.

to the front surface of the thin c-Si substrate, a significant absorption loss is still observed at wavelengths greater than 900 nm. This absorption loss is due to the insufficient thickness of the c-Si for effective light absorption in the NIR region, considering the relatively long absorption depth of c-Si for NIR light (Figure 1B). To mitigate the absorption loss of the NIR wavelengths, the RIP-PDMS film was also applied to the rear surface of the thin c-Si layer. The textured surface of the RIP-PDMS was coated with a 300-nm-thick metal layer to fabricate the RIP-PDMS

film in the form of an attachable diffuse mirror, as shown in Figure S4. By attaching the diffuse mirror on the rear surface of the thin c-Si layer, the NIR light could be recycled with higher diffusion angles than that achieved with a planar metal mirror, and thus, the NIR absorption of the thin c-Si is significantly enhanced, as shown in Figure 2A. Moreover, the integrated photon flux of the thin c-Si with RIP-PDMS films on both surfaces increased from 82.1% to 85.4% compared to that of the thin c-Si with an RIP-PDMS film only on the front surface (Figure 2B).

To elucidate the mechanism of the absorption enhancement in the thin c-Si with the RIP-PDMS films on its surfaces, we simulated the absorption spectra and integrated photon flux of the same structures with and without the RIP-PDMS films by FDTD simulations (Figures 2B and S5). The results of FDTD simulations are consistent with the experimentally obtained values, once again confirming that the light absorption of the thin c-Si increases significantly over a broad wavelength range with the attachment of the RIP-PDMS film on the front surface. In addition, we observed that the NIR absorption of the thin c-Si increased further upon the attachment of an RIP-PDMS film as a rear-surface diffuse mirror. The simulated integrated photon flux of the thin c-Si increases from 78.1% to 82.5% with the attachment of the RIP-PDMS film on its front surface and increases further from 82.5% to 87.1% with the attachment of an additional RIP-PDMS film on the rear surface. Vertical cross-sections of the time-averaged Poynting vectors of the NIR light (λ = 1,000 nm) through the thin c-Si with and without RIP-PDMS films were compared (Figure 2C). The time-averaged Poynting vector ($\langle S \rangle$) represents the power flow near the structure. The Poynting vector analysis not only indicates that the interacting NIR light is more diffused inside the thin c-Si with RIP-PDMS films on both surfaces but also indicates that a larger amount of the solar energy in the NIR region can be trapped and absorbed by the thin c-Si, owing to the enhanced light diffusion, than that can be achieved with the flat c-Si (non-textured) without RIP-PDMS films. To confirm the enhanced light diffusion facilitated by the RIP-PDMS films, far-field projections of the NIR light were monitored inside the c-Si immediately after front-surface refraction and rear-surface diffuse reflection by the RIP-PDMS films, respectively (Figure 2D). The averaged half-angle of the NIR light, monitored inside the c-Si, increases to 10°, owing to refraction by the RIP-PDMS film on the front surface (see Figure S6) and to 15° by diffuse reflection by the RIP-PDMS film on the rear surface (see also Figure S7).

Photovoltaic Performance of Thin c-Si Solar Cells with RIP-PDMS Films

To confirm the effect of the RIP-PDMS films, we fabricated flexible photovoltaic devices, as shown in Figure 3A. The thin c-Si solar cells were fabricated based on the conventional doping process that is commercially used for manufacturing c-Si solar cells. To reduce the shading loss and collect the generated carriers effectively, we applied a micro-grid electrode that has a high transmittance of >97% on the front surface of the device.[26] In general, a metal electrode that also acts as a light-reflecting mirror is covered on the rear surface of conventional c-Si solar cells. However, when a metal mirror covers the rear surface of the thin c-Si solar cell, it is not possible to apply the RIP-PDMS film with a back-metal reflector on the rear surface. Therefore, micro-grid electrodes that show both effective carrier collection and high transmittance were formed on both the front and rear surfaces of the thin c-Si solar cells. In addition, because the micro-grid electrode is thin (<500 nm), the RIP-PDMS film can be successfully attached without forming an air gap between the RIP-PDMS film and the thin c-Si solar cell (see Figure S8). As shown in Table 1 and Figure 3B, the planar thin c-Si solar cells without the RIP-PDMS film exhibited a relatively low short-circuit current density (J_{sc}) of 29.6 mA/cm^2, owing to the low light absorption

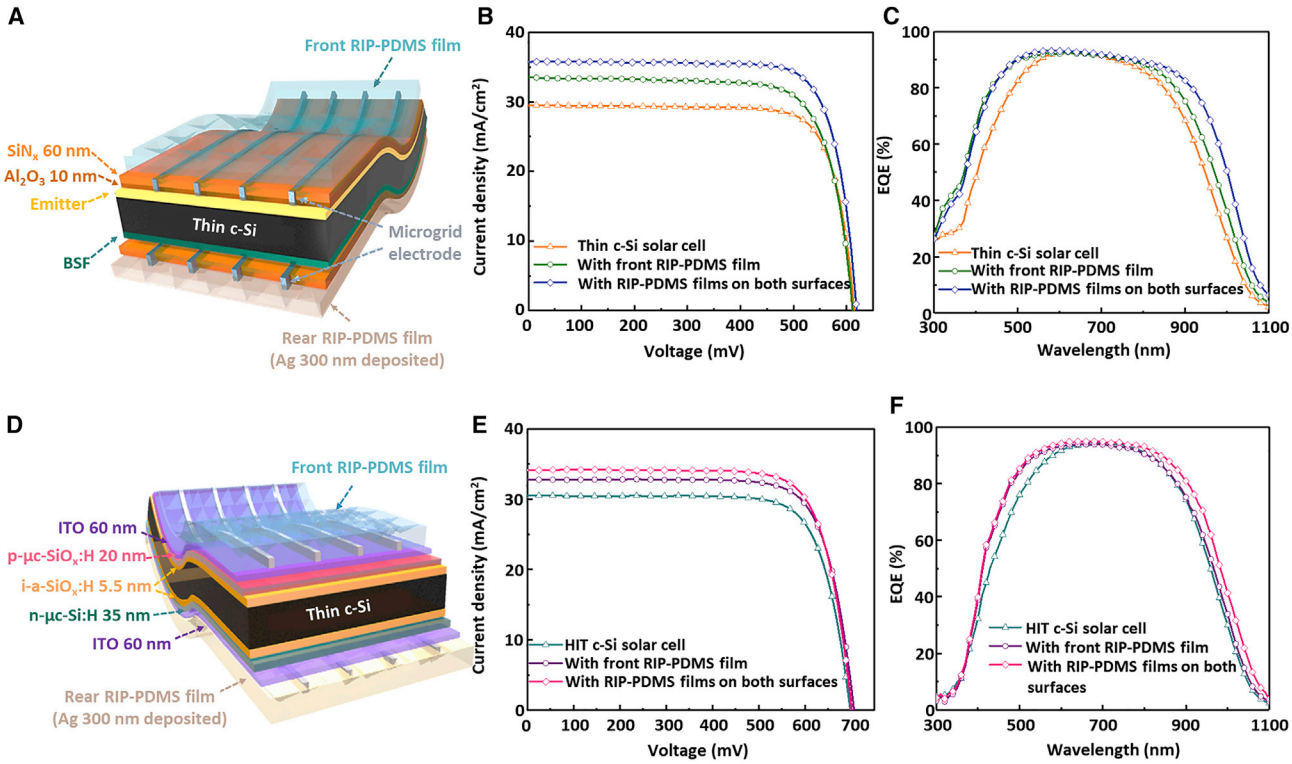

Figure 3. Photovoltaic Performance of Thin c-Si Solar Cells with RIP-PDMS Films

(A) Schematic illustration of a thin c-Si solar cell.

(B) Current density-voltage (*J-V*) characteristics of thin c-Si solar cells with and without RIP-PDMS films.

(C) External quantum efficiency (EQE) curves of thin c-Si solar cells with and without RIP-PDMS films.

(D) Schematic illustration of an HIT thin c-Si solar cell.

(E) *J-V* characteristics of HIT thin c-Si solar cells with and without RIP-PDMS films.

(F) EQE curves of HIT thin c-Si solar cells with and without RIP-PDMS films.

by the cell. As shown in Figure S9 and Table S1, the thin c-Si solar cell with a flat-PDMS film did not show a significant change in average J_{sc}. This indicates that the surface structures on PDMS decrease the surface reflection and increase the optical path length in the c-Si. When the RIP-PDMS film was attached to the front surface of the thin c-Si solar cell, the average J_{sc} value improved to 33.0 mA/cm^2. Furthermore, the thin c-Si solar cell with RIP-PDMS films on both surfaces showed a higher average J_{sc} value of 35.3 mA/cm^2. From Figures 3C and S10, we confirmed that the increased J_{sc} of the thin c-Si solar cell with RIP-PDMS films on both surfaces originated from the improved external quantum efficiency (EQE) at wavelengths greater than 900 nm compared to the thin c-Si solar cell with only the front RIP-PDMS film. As shown in Figure S10, the reflectance spectra of the thin c-Si solar cells decreased when a RIP-PDMS film was attached to the rear side. Hence, light passing through the thin c-Si solar cells is diffused by the rear RIP-PDMS film, resulting in an increase in the optical path length, as shown in Figures 2C and 2D (FDTD simulation). Therefore, the EQE response at long wavelengths was further increased due to the increased optical path length in the presence of the rear RIP-PDMS film. Considering that the other photovoltaic parameters, such as the fill factor (FF) and open-circuit voltage (V_{oc}), remain constant, because the RIP-PDMS films were physically attached onto the thin c-Si solar cells, the thin c-Si solar cell with RIP-PDMS films on both surfaces showed a maximum efficiency of 17.3% (V_{oc} = 618 mV, J_{sc} = 35.8 mA/cm^2, and FF = 78.3%).

Table 1. Device Performance of Thin c-Si Solar Cells with and without RIP-PDMS Films

Device	J_{sc} (mA/cm^2)	V_{oc} (mV)	FF (%)	Efficiency (%)
Thin c-Si solar cells	29.6 ± 0.3 (30.1)	617 ± 3.0 (618)	77.9 ± 0.2 (77.9)	14.3 ± 0.1 (14.5)
With RIP-PDMS on the front surface	33.0 ± 0.5 (32.5)	616 ± 4.0 (618)	77.2 ± 1.3 (78.7)	15.5 ± 0.3 (15.8)
With RIP-PDMS on both surfaces	35.3 ± 0.6 (35.8)	618 ± 0.0 (618)	77.6 ± 0.5 (78.3)	16.9 ± 0.3 (17.3)

Average value obtained from ten devices. The values in brackets are obtained from the champion device. The error range represents the standard deviation.

Thus, attaching an RIP-PDMS film through a simple physical process effectively increased the light absorption capability of the thin c-Si layer, implying that the RIP-PDMS film can be applied universally to various types of flexible solar cells to enhance their light absorption capability. To confirm this, we fabricated HIT-based thin c-Si solar cells (see Figure 3D for a schematic). The HIT thin c-Si solar cell with high-quality intrinsic amorphous Si (a-Si) passivation enables significant improvement in V_{oc}.[27] As shown in Figure 3E and Table 2, the HIT thin c-Si solar cell showed a significantly improved V_{oc} of >700 mV than that of the doping-processed thin c-Si solar cells (V_{oc} = 618 mV). As expected, the HIT thin c-Si solar cell with RIP-PDMS films on both surfaces exhibited a maximum efficiency of 18.4% (V_{oc} = 709 mV, J_{sc} = 34.3 mA/cm^2, and FF = 76.3%), which is significantly higher than that of a device without the RIP-PDMS film (16.3%). However, the EQE response in the short-wavelength region (300–400 nm) did not improve compared with that of the doping-processed thin c-Si solar cell (Figure 3F) because of the parasitic absorption of light by the indium tin oxide (ITO) electrode and a-Si layers.[28] As a result, the average J_{sc} value of the HIT thin c-Si solar cell with RIP-PDMS films (34.3 mA/cm^2) is slightly lower than that of the doping-processed thin c-Si solar cell with RIP-PDMS films (35.3 mA/cm^2). As shown in Figure S11 and Table S2, our devices showed outstanding performance compared to recently reported thin c-Si flexible solar cells.

Flexible and Angle-Dependent Photovoltaic Performance of Thin c-Si Solar Cells with RIP-PDMS Films

The photovoltaic properties of the conventional doping-processed thin c-Si solar cell with RIP-PDMS films were evaluated during repeated bending deformation to confirm its flexibility and stable efficiency. The device was repeatedly bent (1,000 times) at an $R_{bending}$ of 5 mm (bending speed, 300 mm/min). The RIP-PDMS films did not peel off the thin c-Si solar cell during the repeated bending test because of its elasticity and excellent adhesion to the cell.[20,24,25] Although the thin c-Si solar cell with RIP-PDMS films on both surfaces was repeatedly bent for 1,000 cycles, impressively, all photovoltaic parameters, such as V_{oc}, J_{sc}, FF, and the overall

Table 2. Device Performance of HIT Thin c-Si Solar Cells with and without the RIP-PDMS Films

Device	J_{sc} (mA/cm^2)	V_{oc} (mV)	FF (%)	Efficiency (%)
HIT thin c-Si solar cells	30.7 ± 0.3 (30.3)	673 ± 16 (699)	76.3 ± 1.8 (77.1)	15.8 ± 0.7 (16.3)
With RIP-PDMS on the front surface	33.2 ± 0.2 (33.2)	676 ± 20 (709)	75.9 ± 1.7 (76.6)	17.0 ± 0.8 (18.0)
With RIP-PDMS on both surfaces	34.3 ± 0.3 (34.1)	680 ± 17 (709)	75.4 ± 1.8 (76.3)	17.5 ± 0.7 (18.4)

Average value obtained from eight devices. The values in brackets are obtained from the champion device. The error range represents the standard deviation.

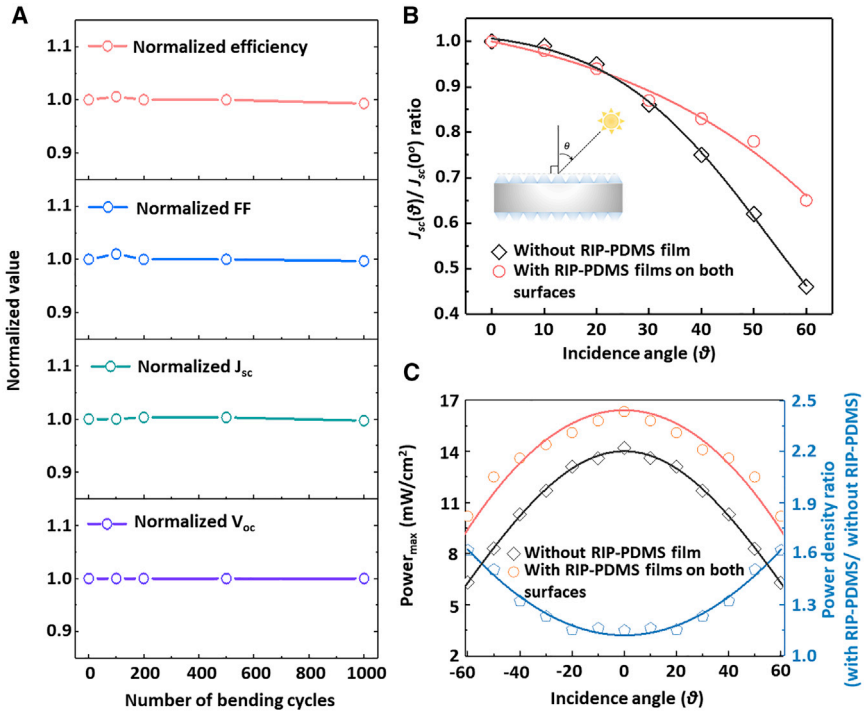

Figure 4. Flexible and Angle-Dependent Photovoltaic Performance of Thin c-Si Solar Cells with RIP-PDMS Films

(A) Normalized values of J_{sc}, V_{oc}, FF, and efficiency as functions of the bending cycle.

(B) Relative J_{sc}, ratio, with respect to J_{sc}, at normal incidence, for different light incidence angles for cells with and without the RIP-PDMS film. Light incidence angle is defined in the inset.

(C) Maximum power density and power density ratio of the thin c-Si solar cells with and without the RIP-PDMS film as functions of the incidence angle (right y axis).

efficiency, remained constant (Figure 4A). Moreover, the HIT thin c-Si solar cells with RIP-PDMS films also showed stable photovoltaic properties during repeated bending tests for 1,000 cycles (see Figure S12). The $R_{bending}$ of the HIT thin c-Si solar cell was, however, higher at 10 mm, because of the ITO electrodes used in this cell.[29] In conclusion, the attached RIP-PDMS films do not cause any physical damage to thin c-Si solar cells under repeated bending deformations.

Another advantage of the RIP-PDMS film would be the mitigation of the angle dependency of the incident light absorption by the c-Si layer. Because the position of the sun changes during the day and year, the overall efficiency of solar cells also varies with time. In particular, because flexible solar cells can be installed on mobile devices as continuous energy sources, the generated power may be much lower than the value estimated under normal incidence. To investigate the change in the absorption capability of the thin c-Si solar cell with RIP-PDMS films under various angles of the incident light, its J_{sc} was measured by tilting the device from 0° to 60°, as shown in Figure S13. The relative J_{sc} ratio of the thin c-Si solar cell with RIP-PDMS films increased continuously compared with that of the same device without the RIP-PDMS film, with the increase in the angle of the incident light (Figure 4B). Notably, at an incident angle of 60°, the relative J_{sc} ratio is much higher for the thin c-Si solar cell with the RIP-PDMS films (0.65) than that for the device without the RIP-PDMS film (0.45). Because of the strong light scattering and anti-reflection properties of the RIP-PDMS film, the thin c-Si solar cell with the RIP-PDMS film showed a smaller reduction in the J_{sc} ratio with increasing angle of light incidence

compared with that of the device without the film.[30] As a result, the maximum power density of the thin c-Si solar cell with RIP-PDMS films is consistently higher than that of the device without the RIP-PDMS film at all incident angles between 0° and 60°. Furthermore, the power density ratio between the thin c-Si solar cell with and without the RIP-PDMS films increased from 1.14 to 1.62 at an incident angle of 60°. Thus, the RIP-PDMS film can effectively mitigate the light absorption loss of the thin c-Si flexible solar cells under the high angle of light incidence (Figure 4C).

DISCUSSION

In conclusion, we developed highly efficient 20-μm-thin c-Si flexible solar cells that show stable flexibility and high light absorption capability by employing RIP-PDMS films. The RIP-PDMS film increases the integrated photon flux absorption of the thin c-Si from 75.0% to 85.4%. FDTD simulations confirm that the light absorption by the thin c-Si with RIP-PDMS film increased because the angles of the incident light at the front and rear surfaces of the thin c-Si tilted up to 10° and 15°, respectively. Owing to the increased angles of the refracted light, the optical path length of the thin c-Si is higher, resulting in improved absorption properties. As a result, we achieved a thin c-Si flexible solar cell with a remarkable efficiency of 18.4% by applying the RIP-PDMS films on both the front and rear surfaces of the thin c-Si solar cell. Moreover, the thin c-Si solar cell with the RIP-PDMS film showed constant photovoltaic parameters during 1,000 cycles of a bending test with a bending radius of <10 mm. Thus, the use of RIP-PDMS films is expected to serve as a new strategy for the fabrication of highly efficient thin c-Si flexible solar cells.

EXPERIMENTAL PROCEDURES

Resource Availability

Lead Contact

Further information and requests for resources should be directed to and will be fulfilled by the lead contact, Kwanyong Seo, kseo@unist.ac.kr.

Materials Availability

This study did not generate new unique reagents.

Data and Code Availability

The authors declare that the data supporting the findings of this study are available within the article and the Supplemental Information. All other data are available from the lead contact upon reasonable request.

Fabrication of Random Inverted-Pyramidal PDMS Films

To fabricate a micro-pyramid-structured silicon mold, a planar c-Si substrate was first cleaned with acetone, methanol, and de-ionized (DI) water. After the native silicon oxide was removed by immersing in a buffered oxide etchant, the planar silicon substrate was dried with N_2 gas. The cleaned silicon substrate was then immersed in a wet-etching solution of potassium hydroxide (KOH):isopropyl alcohol (IPA):DI water = 1:0.5:8.5 vol % at 75°C for 40 min to fabricate the random size pyramid-structured silicon mold. To remove the remaining potassium ions on the silicon substrate, a solution of hydrochloric acid (HCl):hydroperoxide (H_2O_2):H_2O = 1:1:5 was used at 80°C for 10 min. Next, a monolayer of trichloro-(1H,1H,2H,2H-perfluorooctyl)silane was deposited to detach the textured PDMS layer easily. A mixed solution of the PDMS base resin and curing agent (Sylgard 184, Dow Corning) was poured on the silicon master mold and annealed at 100°C for 10 min. Finally, the cured RIP-PDMS film was detached from the silicon master mold.

Fabrication of Thin c-Si Solar Cells

The Czochralski (Cz) grade n-type c-Si wafers (resistivity, 1–3 Ω cm; thickness, 380 μm) were etched in a KOH etching solution at 80°C to fabricate thin c-Si substrates (20 μm). To remove the remaining potassium ions on the thin c-Si substrate, a piranha solution (H_2SO_4:H_2O_2 = 4:1 volume ratio) was used at 80°C for 10 min. The emitter and the back-surface-field (BSF) layers were formed by the spin-on-dopant (SOD) method. First, a phosphorus source (P509, Filmtronics) was spin coated on a dummy Si wafer and then it was baked at 200°C for 20 min to remove the organic solvent. The rear surface of the thin c-Si substrate was positioned to face the P509-coated dummy wafer to form a BSF layer. The diffusion doping was carried out in a tube furnace under a mixed ambient of O_2 (125 sccm) and N_2 (500 sccm) at 900°C. The phosphorus silicate glass formed after the SOD diffusion process was removed with a buffered oxide etchant. After removing the phosphorus silicate glass, an emitter layer was formed using a boron source (B155, Filmtronics). The B155 solution was spin coated on a dummy Si wafer and then it was baked at 200°C for 20 min. To form the conformal emitter layer, the front surface of the thin c-Si substrate was positioned to face the B155-coated dummy wafer. The diffusion doping process was carried out in a tube furnace under 500 sccm N_2 at 880°C. A thin Al_2O_3 layer (10 nm in thickness) used as a passivation layer was deposited by atomic layer deposition (atomic premium, CN1). After the deposition of the Al_2O_3 passivation layer, SiN_x was deposited on the front (60 nm) and rear surfaces (100 nm) of the thin c-Si substrate. To fabricate the top and bottom micro-grid electrodes, the front and rear surfaces of the thin c-Si solar cells were patterned by a photolithography process using an AZ4330 photoresist (AZ electronic materials). As top and bottom electrodes, 500- and 200-nm-thick Al films were deposited on the top and bottom of the samples, respectively, using a thermal evaporator. Finally, the photoresist residue was removed with acetone. The active area of the flexible solar cell is 1 cm^2.

Fabrication of HIT Thin c-Si Solar Cells

The Cz grade n-type c-Si wafers (resistivity, 1–3 Ω cm; thickness, 380 μm) were etched in a KOH etching solution at 80°C to fabricate thin c-Si substrates (20 μm). To remove the remaining potassium ions on the thin c-Si substrate, a piranha solution (H_2SO_4:H_2O_2 = 4:1 volume ratio) was used at 80°C for 10 min. Before the deposition of the intrinsic hydrogenated amorphous silicon oxide (i-a-SiO_x:H) passivation layer, the c-Si wafer was dipped in a 1% to 2% hydroflouric acid (HF) solution to remove the native oxide. After the HF treatment, a 5.5-nm-thick i-a-SiO_x:H passivation layer was deposited on both sides of the c-Si substrate by very high frequency (VHF)-plasma enhanced chemical vapor deposition (PECVD) at an excited frequency of 60 MHz. A mixture of SiH_4, H_2, and CO_2 (1.4, 10.5, and 0.74 sccm, respectively) was used as the source gas. The deposition pressure, substrate temperature, and VHF power were set as 40 Pa, 165°C, and 1 W, respectively. For preparing the p- and n-type layers, p-type hydrogenated microcrystalline silicon oxide (p-μc-SiO_x:H) deposited by VHF-PECVD and n-type hydrogenated microcrystalline silicon (n-μc-Si:H) deposited by radio frequency (RF)-PECVD, respectively, were used. The thickness of the p- and n-type layer was 20 nm and 35 nm, respectively. For the deposition of p-μc-SiO_x:H, the flow rates of SiH_4, H_2, CO_2, and B_2H_6 were fixed at 2.5, 261, 0.4, and 0.003 sccm, respectively. The deposition pressure, substrate temperature, and VHF power were set as 100 Pa, 170°C, and 20 W, respectively. For the deposition of n-μc-Si:H, the flow rates of SiH_4, H_2, and PH_3 were fixed at 3.7, 301, and 0.016 sccm, respectively. The deposition pressure, substrate temperature, and RF power were set as 200 Pa, 170°C, and 10 W, respectively. After the deposition of the silicon-based layers, thermal annealing in forming gas (3% H_2 in N_2) was carried out to improve the passivation quality. The annealing temperature and duration were set as 225°C and 5 min, respectively. After the thermal annealing process, an ITO film of 60 nm was deposited on the p-μc-SiO_x:H

layer and n-μc-Si:H layer by RF magnetron sputtering using an ITO target (SnO_2:In_2O_3 = 1:9) with a diameter of 80 mm. The flow rate of Ar, sputtering pressure, and sputtering power were set as 14.2 sccm, 0.5 Pa, and 50 W, respectively. The sputtering of ITO was carried out without heating the substrate. To serve as top and bottom electrodes, 500- and 200-nm-thick Al films were deposited on the top and bottom of the samples, respectively, using a thermal evaporator. Finally, the photoresist residue was removed with acetone. The active area of the fabricated flexible solar cell is 1 cm^2.

Attachment of the RIP-PDMS Film to the Thin c-Si Solar Cell

Before attaching the RIP-PDMS film to the thin c-Si solar cell, the surface of the solar cells was cleaned with IPA. If there is dust or particles on the surface of the thin c-Si solar cell, an air gap can be formed between the RIP-PDMS film and the thin c-Si solar cell, which can reduce the light absorption of the solar cell. To further ensure that an air gap was not formed, we started attaching the RIP-PDMS film at the edge of the thin c-Si solar cell, rather than at the center of the device.

Characterization of the Photovoltaic Properties

The photovoltaic properties of the solar cells were evaluated using an Oriel Sol3A Class AAA solar simulator (Newport) under AM 1.5G illumination. The incident flux was confirmed by a calibrated power meter and double checked using a National Renewable Energy Laboratory (NREL)-calibrated solar cell (PV Measurements). EQE spectra were recorded in the wavelength range of 300–1,100 nm using a Xe light source and a monochromator. Optical reflections of the samples were measured with a UV-vis-NIR spectrophotometer (Cary 5000, Agilent) equipped with a 110-mm integrating sphere to collect the total light (diffuse and specular) reflected from the samples.

Bending Test

To evaluate the mechanical flexibility of the thin c-Si solar cells, a custom-built bending test system was used. The efficiency of the flexible devices was evaluated under bending deformation.

FDTD Simulations

The FDTD simulation was carried out using the commercial FDTD software package Lumerical FDTD Solution 8.15. For this, 7 × 7 μm^2 periodic boundary conditions (x, y direction) and 30 × 30 × 10 nm^3 uniform mesh were used to account for the absorption and light behavior of 20-μm-thin c-Si. The incident light in the wavelength range of 300–1,400 nm was irradiated at a normal incidence angle. The design of the RIP-PDMS film was described using the scanning electron micrographs of the film. In addition, to describe the real structure of the RIP-PDMS film, 13 different-sized pyramids (depth: 2–6 μm) were used. Refractive indexes (n, k) reported by Shinke (c-Si),[31] Philipp (SiN_x),[32] and Palik (Ag)[33] were used to describe the experimental absorption spectra.

SUPPLEMENTAL INFORMATION

Supplemental Information can be found online at https://doi.org/10.1016/j.xcrp.2020.100242.

ACKNOWLEDGMENTS

This work was supported by the New Renewable Energy Core Technology Development Project of the Korea Institute of Energy Technology Evaluation and Planning (KETEP) granted financial resource from the Ministry of Trade, Industry and Energy, Republic of Korea (no. 20183010013900). It was also supported by the National Research Foundation of Korea (NRF) grant funded by the Korean Government (MSIP) (NRF-

2017M1A2A2087812, NRF-2018R1D1A1B07051197, NRF-2019R1A2C2086602, NRF-2019M1A2A2065614, and NRF-2020R1A4A2002590). This work also was supported by the 2020 Research Fund (1.200092.01) of UNIST (Ulsan National Institute of Science and Technology).

AUTHOR CONTRIBUTIONS

I.H. and Y.J. contributed equally to this work. I.H., Y.J., I.Y., and K.S. designed the experiment. I.H. and Y.S. carried out the device fabrication. Y.S. and S.M. guided and helped the fabrication of the HIT thin c-Si solar cells. I.H. and J.P. carried out the optical microscope imaging and optical measurement. Y.J. and I.Y. performed FDTD simulation. I.Y. and K.S. supervised the whole project. All authors contributed to the discussion and interpretation of the results and completion of the manuscript.

DECLARATION OF INTERESTS

The authors declare no competing interests.

Received: July 16, 2020
Revised: September 11, 2020
Accepted: September 30, 2020
Published: November 4, 2020

REFERENCES

1. Battaglia, C., Cuevas, A., and De Wolf, S. (2016). High-efficiency crystalline silicon solar cells: status and perspectives. Energy Environ. Sci. *9*, 1552–1576.

2. Hwang, I., Um, H.-D., Kim, B.-S., Wober, M., and Seo, K. (2018). Flexible crystalline silicon radial junction photovoltaics with vertically aligned tapered microwires. Energy Environ. Sci. *11*, 641–647.

3. Hadibrata, W., Es, F., Yerci, S., and Turan, R. (2018). Ultrathin Si solar cell with nanostructured light trapping by metal assisted etching. Sol. Energy Mater. Sol. Cells *180*, 247–252.

4. Wang, S., Weil, B.D., Li, Y., Wang, K.X., Garnett, E., Fan, S., and Cui, Y. (2013). Large-area free-standing ultrathin single-crystal silicon as processable materials. Nano Lett. *13*, 4393–4398.

5. Zhou, S., Yang, Z., Gao, P., Li, X., Yang, X., Wang, D., He, J., Ying, Z., and Ye, J. (2016). Wafer-scale integration of inverted nanopyramid arrays for advanced light trapping in crystalline silicon thin film solar cells. Nanoscale Res. Lett. *11*, 194.

6. Yu, K.J., Gao, L., Park, J.S., Lee, Y.R., Corcoran, C.J., Nuzzo, R.G., Chanda, D., and Rogers, J.A. (2013). Light trapping in ultrathin monocrystalline silicon solar cells. Adv. Energy Mater. *3*, 1401–1406.

7. Pagliaro, M., Ciriminna, R., and Palmisano, G. (2008). Flexible solar cells. ChemSusChem *1*, 880–891.

8. Wang, K.X., Yu, Z., Liu, V., Cui, Y., and Fan, S. (2012). Absorption enhancement in ultrathin crystalline silicon solar cells with antireflection and light-trapping nanocone gratings. Nano Lett. *12*, 1616–1619.

9. Yan, W., Tao, Z., Gu, M., and Richards, B.S. (2017). Photocurrent enhancement of ultrathin front-textured crystalline silicon solar cells by rear-located periodic silver nanoarrays. Sol. Energy *150*, 156–160.

10. Zhang, J., Zhang, Y., Song, T., Shen, X., Yu, X., Lee, S.T., Sun, B., and Jia, B. (2017). High-performance ultrathin organic-inorganic hybrid silicon solar cells via solution-processed interface modification. ACS Appl. Mater. Interfaces *9*, 21723–21729.

11. Aurang, P., Turan, R., and Unalan, H.E. (2017). Nanowire decorated, ultra-thin, single crystalline silicon for photovoltaic devices. Nanotechnology *28*, 405205.

12. Branham, M.S., Hsu, W.C., Yerci, S., Loomis, J., Boriskina, S.V., Hoard, B.R., Han, S.E., and Chen, G. (2015). 15.7% Efficient 10-μm-thick crystalline silicon solar cells using periodic nanostructures. Adv. Mater. *27*, 2182–2188.

13. Jeong, S., McGehee, M.D., and Cui, Y. (2013). All-back-contact ultra-thin silicon nanocone solar cells with 13.7% power conversion efficiency. Nat. Commun. *4*, 2950.

14. Oh, J., Yuan, H.C., and Branz, H.M. (2012). An 18.2%-efficient black-silicon solar cell achieved through control of carrier recombination in nanostructures. Nat. Nanotechnol. *7*, 743–748.

15. Woo, J.-H., Kim, Y.-C., Kim, S.-H., Jang, J., Han, H.N., Choi, K.J., Kim, I., and Kim, J.-Y. (2017). Critical bending radius of thin single-crystalline silicon with dome and pyramid surface texturing. Scr. Mater. *140*, 1–4.

16. Blakers, A.W., and Armour, T. (2009). Flexible silicon solar cells. Sol. Energy Mater. Sol. Cells *93*, 1440–1443.

17. Pathi, P., Peer, A., and Biswas, R. (2017). Nano-photonic structures for light trapping in ultra-thin crystalline silicon solar cells. Nanomaterials (Basel) *7*, 17.

18. Andreani, L.C., Bozzola, A., Kowalczewski, P., Liscidini, M., and Redorici, L. (2019). Silicon solar cells: toward the efficiency limits. Adv. Phys. X *4*, 1548305.

19. Lochtefeld, A., Wang, L., Carroll, M., Han, J., Stryker, D., Bengtson, S., Yao, Y., Lin, D., Ji, J., Leitz, C., et al. (2013). 15%, 20 micron thin, silicon solar cells on steel. 2013 IEEE 39th Photovoltaic Specialists Conference (PVSC) (IEEE), pp. 1364–1365.

20. Hwang, I., Choi, D., Lee, S., Seo, J.H., Kim, K.H., Yoon, I., and Seo, K. (2017). Enhancement of light absorption in photovoltaic devices using textured polydimethylsiloxane stickers. ACS Appl. Mater. Interfaces *9*, 21276–21282.

21. Lee, S.G., Lee, D.Y., Lim, H.S., Lee, D.H., Lee, S., and Cho, K. (2010). Switchable transparency and wetting of elastomeric smart windows. Adv. Mater. *22*, 5013–5017.

22. Kang, S.M., Ahn, N., Lee, J.-W., Choi, M., and Park, N.-G. (2014). Water-repellent perovskite solar cell. J. Mater. Chem. A *2*, 20017–20021.

23. Lin, S., Ai, L., Zhang, J., Bu, T., Li, H., Huang, F., Zhang, J., Lu, Y., and Song, W. (2019). Silver ants-inspired flexible photonic architectures with improved transparency and heat radiation for photovoltaic devices. Sol. Energy Mater. Sol. Cells *203*, 110135.

24. Kroner, E., Maboudian, R., and Arzt, E. (2010). Adhesion characteristics of PDMS surfaces during repeated pull-off force measurements. Adv. Eng. Mater. *12*, 398–404.

25. Jeong, S.H., Zhang, S., Hjort, K., Hilborn, J., and Wu, Z. (2016). PDMS-based elastomer tuned soft, stretchable, and sticky for epidermal electronics. Adv. Mater. *28*, 5830–5836.

26. Um, H.-D., Hwang, I., Kim, N., Yu, Y.J., Wober, M., Kim, K.-H., and Seo, K. (2015). Microgrid electrode for Si microwire solar cells with a fill factor of over 80%. Adv. Mater. Interfaces *2*, 1500347.

27. Mishima, T., Taguchi, M., Sakata, H., and Maruyama, E. (2011). Development status of high-efficiency HIT solar cells. Sol. Energy Mater. Sol. Cells *95*, 18–21.

28. Holman, Z.C., Descoeudres, A., Barraud, L., Fernandez, F.Z., Seif, J.P., De Wolf, S., and Ballif, C. (2012). Current losses at the front of silicon heterojunction solar cells. IEEE J. Photovolt. *2*, 7–15.

29. Zhinong, Y., Longfeng, X., Wei, X., and Huaqing, W. (2007). The bending properties of flexible ITO films. 2007 Asia Optical Fiber Communication and Optoelectronics Conference (IEEE), pp. 148–150.

30. Takumi, T., Lloyd, S., Murata, H., and Vohra, V. (2019). Low-cost light manipulation coatings for polymer solar cell photocurrent increase under various incident angles. Mater. Res. Lett. *7*, 68–74.

31. Schinke, C., Christian Peest, P., Schmidt, J., Brendel, R., Bothe, K., Vogt, M.R., Kröger, I., Winter, S., Schirmacher, A., Lim, S., et al. (2015). Uncertainty analysis for the coefficient of band-to-band absorption of crystalline silicon. AIP Adv. *5*, 067168.

32. Philipp, H.R. (1973). Optical properties of silicon nitride. J. Electrochem. Soc. *120*, 295–300.

33. Philipp, H. (1997). Silicon nitride (Si3N4)(noncrystalline). In Handbook of Optical Constants of Solids, E.D. Palik, ed. (Elsevier), pp. 771–774.